IEEE Access
Multidisciplinary | Rapid Review | Open Access Journal

Received December 18, 2019, accepted December 31, 2019, date of publication January 6, 2020, date of current version January 15, 2020.

Digital Object Identifier 10.1109/ACCESS.2020.2964010

Design of a 3-DOF Parallel Manipulator to Compensate for Disturbances in Facade Cleaning

GARAM PARK[1], JOOYOUNG HONG[2], SUNGKEUN YOO[2], HWA SOO KIM[3], (Member, IEEE), AND TAEWON SEO[1], (Member, IEEE)

[1]School of Mechanical Engineering, Hanyang University, Seoul 04763, South Korea
[2]School of Mechanical and Aerospace Engineering, Seoul National University, Seoul 151019, South Korea
[3]Department of Mechanical System Engineering, Kyonggi University, Suwon 16227, South Korea

Corresponding authors: Hwa Soo Kim (hskim94@kgu.ac.kr) and Taewon Seo (taewonseo@hanyang.ac.kr)

This work was supported in part by the National Research Foundation of Korea (NRF) grant funded by the Ministry of Science and ICT for First-Mover Program for Accelerating Disruptive Technology Development under Grant 2018M3C1B9088331 and Grant 2018M3C1B9088332, and in part by the Human Resources Program in Energy Technology of the Korea Institute of Energy Technology Evaluation and Planning (KETEP)-granted financial resource from the Ministry of Trade, Industry and Energy, South Korea, under Grant 20184030201970.

ABSTRACT This paper proposes a three-degree-of-freedom manifold composed of three linear actuators. The proposed mechanism consists of a workspace suitable for facade cleaning and can compensate for the horizontal position from disturbances in a gondola-based exterior-wall cleaning. We design a cleaning manipulator that can ensure a constant cleaning area by compensating for the disturbance in each direction. The position, velocity kinematic, and Jacobian-based singularity analysis are presented, and kinematic variables are defined to extend a singularity-free workspace. In addition, optimization is performed based on an index that demonstrates the mechanical properties of the manipulator. The result shows how the manipulator compensates for the disturbances as well as the features of the optimization model. This study can be applied to robot manipulators for facade cleaning in the future.

INDEX TERMS Kinematics, optimal design, parallel mechanism, 3-DOF, workspace.

I. INTRODUCTION

As the number of high-rise buildings increases, maintaining and cleaning the exterior walls of buildings have become important. Solutions such as the GEKKO facade robot of SERBOT in Switzerland, SIRIUS facade-cleaning robot of Fraunhofer, and SkyPro facade cleaner in Cyprus [1]–[3] have been presented as applications for facade cleaning. However, Figure 1 shows that to ensure a constant area for cleaning of high-rise buildings under frequent swinging due to wind, resisting or compensating for horizontal directional shaking is necessary. Among the existing solutions, robots mounted on a gondola or hung from the upper part of the building suffer from the limitation in that they cannot compensate for the horizontal shaking due to wind [4]–[6]. In some cases, the gondola has a vertical linear guide to maintain the lateral directional disturbance; however small lateral directional error is very critical to the cleaning performance to fail the cleaning operation [7]–[9].

The associate editor coordinating the review of this manuscript and approving it for publication was Jinguo Liu.

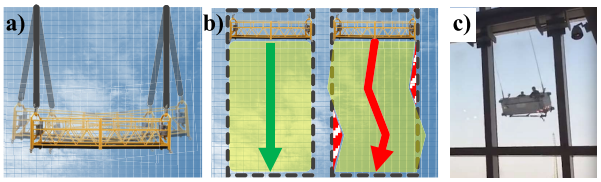

FIGURE 1. Horizontal disturbance of the gondola. a) Horizontal shaking of the gondola. b) Interrupted cleaning area. c) Excessive horizontal movement of the gondola and with workers [23].

Solutions such as fixing the position of the robot using air suction [10] and installing a rail at the outer wall of a building [11] are capable of horizontal compensation or can resist shaking. However, the air-suction method suffers from the limitation in that it is less efficient compared with the gondola-mounted parallel manipulator because of its slower cleaning speed. The model that requires the use of rails is limited by the shape of the building, or installing the rails before cleaning is troublesome. A facade-cleaning robot is designed to solve such efficiency and versatility problems.

This work is licensed under a Creative Commons Attribution 4.0 License. For more information, see http://creativecommons.org/licenses/by/4.0/

Joo et al. proposed a two-degree-of-freedom (2-DOF) parallel mechanism with one translational and one rotational DOF through two linear actuations [12]. This mechanism ensures a workspace that is free of singular positions and has high rigidity. It also solves the problems in the previous solutions, namely, low efficiency and inability to apply to various buildings. However, this mechanism suffers from the limitation in that it cannot compensate for the horizontal disturbance of the gondola because it only has two DOFs.

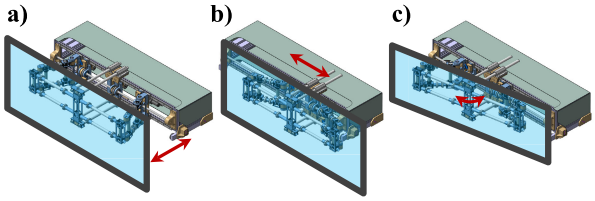

FIGURE 2. Horizontal disturbance compensation during shaking. a) Exact position. b) Compensation for the left horizontal-direction disturbance. c) Compensation for the right horizontal-direction disturbance.

Figure 2 shows our designed three-DOF (3-DOF) parallel manipulator that can compensate for horizontal disturbance during facade cleaning. This mechanism can adjust the topology according to the workspace required for cleaning. The cleaning module attached at the front of the manipulator can be moved by 3-DOF to maintain a constant distance to various types of exterior walls and disturbances of buildings. It also offers the advantage of structural simplicity and reduced weight by moving all the actuators on a single ball screw without any redundancy. Optimization of the kinematic parameters of the manipulator is required to obtain a structure that can be adapted to various workspaces.

Other studies on workspace optimization of a parallel manipulator have been conducted by several researchers. Our study on the method of securing a wide workspace without singularity or analyzing a workspace that changes according to the mechanism was referred from the following works. Kamada et al. have studied a four-DOF parallel mechanism with a wide translational and rotational workspace [13]. Wen et al. proposed a parallel robot using redundancy to ensure that the gripper of the end effector has a large workspace [14]. Liu et al. introduced various work areas according to the change in the link topology using kinematics, singularity, and workspace analysis of a 5R symmetrical parallel mechanism [15]. Li and Xu derived the kinematic manipulability and workspace using kinematic analysis of a 3-PRS parallel manipulator [16]. A parallel mechanism that secures a workspace without singularity was implemented by Gosselin et al. in a 3-DOF manipulator with redundancy using four actuators [17].

For the kinematics of our optimization methodology, we used the methods presented in the following papers.reak Tsai et al. derived the optimal workspace of a 3-UPU parallel manipulator using kinematic optimization [18]. Wu et al. applied kinematic optimization of 3-DOF redundantly planar parallel manipulators to develop hybrid machine tools [19]. Michael and Karol analyzed the optimal workspace of a mechanism applied to a linear delta robot using kinematic optimization of a spatial parallel manipulator [20].

In the design of the robot mechanism, we investigated the structures proposed in the following studies. Harada and Liu proposed a 3-DOF redundantly parallel mechanism to position four actuators on one axis as well as for analysis using an axial-force sensor [21]. Liu *et al.* proposed a new 2-DOF parallel manipulator mechanism and presented a workspace based on kinematic analysis [22].

The objective of the research is to design a manipulator which can compensate the 3-DOF disturbances during façade cleaning operation. To satisfy the requirements for façade cleaning, a novel 3-DOF parallel manipulator with three linear actuators is proposed. The kinematic parameters are optimized to maximize the workspace with high manipulability and no singularity. Position and velocity kinematics are derived to analyze the manipulator. Prototype is developed to test the performance of the manipulator, and successfully verify the compensating capability of the 3-DOF disturbances.

This paper is organized as follows. Section II describes the kinematics of the mechanism. Based on this kinematic analysis, the theoretical workspace obtained from Jacobian analysis is introduced in Section III. Section IV presents the procedure and results of the optimal workspace of the parallel manipulator by satisfying the non-singular positions. Prototype and experiments are presented in Section V, and Section VI provides the concluding remarks.

II. KINEMATICS OF THE MECHANISM

The proposed mechanism is shown in Figure 3 in which the end effector is connected to the base using three links. The links of both right and left consist of two revolute joints and one prismatic joint. In each link, the prismatic joint connected to the base is actuated by a ball-screw mechanism. The central link between the two links consis qts of two intersecting prismatic joints and a revolute joint. The degree of freedom of this simple planar mechanism can be obtained using the Grübler-Kutzbach Formula:

$$M = 3(N - 1 - j) + \sum_{i-1}^{j} f_i, \tag{1}$$

$$N = 6, \quad j = 7, \quad \sum_{i-1}^{j} f_i = 9, \; M = 3. \tag{2}$$

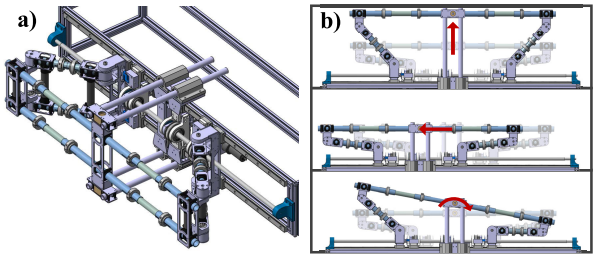

FIGURE 3. Kinematic configuration of the proposed 3-DOF parallel manipulator. a) Architecture of the mechanism. b) Translational and rotational capability of the manipulator.

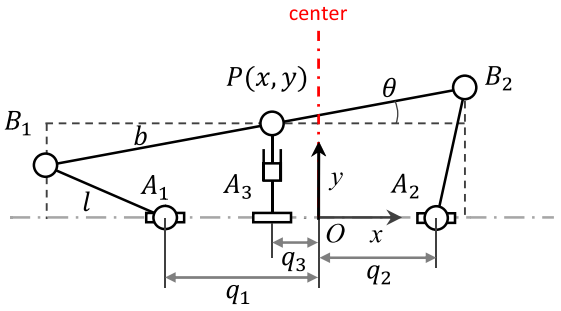

FIGURE 4. Kinematic parameters in terms of the point coordinates.

This configuration can freely move the position of the end effector in an xy plane at angle θ. The kinematic model of the mechanism is shown in Figure 4. The actuated joints are denoted as $A_i(i = 1, 2, 3)$, and the other passive revolute joints are denoted as $B_j(j = 1, 2)$. The end-effector point is denoted as P. The fixed global reference is denoted as the O–xy coordinate. Because the structure of the two mechanisms is symmetrical with respect to the center link, $A_1B_1 = A_2B_2 = l$, $B_1P = B_2P = b$. Each input position of the actuators is denoted as q_i (i=1,2,3).

A. INVERSE KINEMATICS

The position of end-effector point P in the O–xy system can be described by xy coordinate P, i.e.,

$$P = \begin{bmatrix} x & y \end{bmatrix}^T. \tag{3}$$

The positions of two points B_1B_2 can be determined using angle θ and the length of link b, which can be expressed as

$$B_1 = P - \begin{bmatrix} b\cos\theta & b\sin\theta \end{bmatrix}^T = \begin{bmatrix} x - b\cos\theta & y - b\sin\theta \end{bmatrix}^T, \tag{4}$$

$$B_2 = P + \begin{bmatrix} b\cos\theta & b\sin\theta \end{bmatrix}^T = \begin{bmatrix} x + b\cos\theta & y + b\sin\theta \end{bmatrix}^T, \tag{5}$$

where θ is the output angle between the end effector and x axis. The constraint equations are derived as follows:

$$|A_iB_i| = l, \quad i = 1, 2. \tag{6}$$

We can consider each right triangle at both ends of the end effector according to the given length. In this case, by drawing a circle with radius l around both end points, the intersection point with the x axis becomes the position of point A_1,A_2, where the final inverse kinematic equation can be derived as

$$q_1 = x - b\cos\theta \pm \sqrt{l^2 - (y - b\sin\theta)^2}, \tag{7}$$

$$q_2 = x + b\cos\theta \pm \sqrt{l^2 - (y + b\sin\theta)^2}, \tag{8}$$

$$q_3 = x. \tag{9}$$

From Eqs. (7) and (8), four kinematic solutions are available for one fixed position. Note the kinematic solution can be incrementally determined from the previous solution if the manipulator is not passing through singularity. We used the "+−" solution for the manipulation as already shown in Fig. 3. The "+−" configuration can help to reduce the stroke of linear guide in prototype design.

B. JACOBIAN ANALYSIS

Equations (7) and (8) can be differentiated with respect to time to obtain the velocity equations, which yield

$$\begin{aligned}(2b\cos\theta + 2q_1 - 2q_3)\dot{q}_1 + (-2b\cos\theta - 2q_1 + 2q_3)\dot{q}_3 \\ = (2b\sin\theta - 2y)\dot{y} + \{2b\sin\theta(q_1 - q_3) + 2by\cos\theta\}\dot{\theta}\end{aligned} \tag{10}$$

$$\begin{aligned}(2b\cos\theta - 2q_2 + 2q_3)\dot{q}_1 + (-2b\cos\theta + 2q_2 - 2q_3)\dot{q}_3 \\ = (2b\sin\theta + 2y)\dot{y} + \{2b\sin\theta(q_2 - q_3) + 2by\cos\theta\}\dot{\theta}.\end{aligned} \tag{11}$$

Equations (8) and (9) are arranged as follows:

$$\mathbf{A}\dot{\boldsymbol{q}} = \mathbf{B}\dot{\boldsymbol{p}}, \tag{12}$$

where $\dot{q}$ is the vector of the input velocity of each actuator, which is defined as

$$\dot{q} = \begin{bmatrix} \dot{q}_1 & \dot{q}_2 & \dot{q}_3 \end{bmatrix}^T. \tag{13}$$

$\dot{p}$ is the position vector of the output velocity of the end effector, which is defined as

$$\dot{p} = [\dot{x} \quad \dot{y} \quad \dot{\theta}]. \tag{14}$$

The **A** and **B** matrices, which are 3×3 matrices, that describe the relationship between the input and output to control the end effector can be expressed as (15) and (16), shown at the bottom of this page.

The Jacobian matrix is expressed using the relationship of the two preceding matrices as follows:

$$\mathbf{J} = \mathbf{A}^{-1}\mathbf{B}. \tag{17}$$

$$A = \begin{bmatrix} 2b\cos\theta + 2q_1 - 2q_3 & 0 & -2b\cos\theta - 2q_1 + 2q_3 \\ 0 & 2b\cos\theta - 2q_2 + 2q_3 & -2b\cos\theta + 2q_2 - 2q_3 \\ 0 & 0 & 1 \end{bmatrix}, \tag{15}$$

$$B = \begin{bmatrix} 0 & 2b\sin\theta - 2y & 2b\sin\theta(q_1 - q_3) + 2by\cos\theta \\ 0 & 2b\sin\theta + 2y & 2b\sin\theta(q_2 - q_3) + 2by\cos\theta \\ 1 & 0 & 0 \end{bmatrix} \tag{16}$$

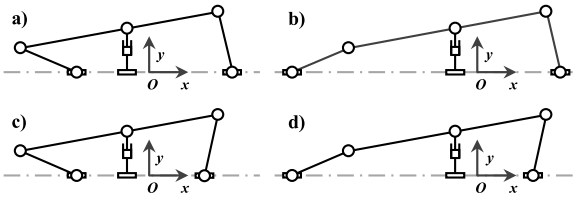

FIGURE 5. Four inverse kinematic models. a) "+ + ++" model. b) "−+" model. c) "+−" model. d) "−−" model.

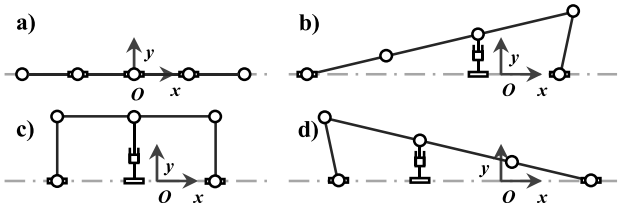

FIGURE 7. Configuration of the singular positions of the manipulator.

III. WORKSPACE ANALYSIS

A. THEORETICAL WORKSPACE

The theoretical workspace is defined as the region where input values q_1, q_2, q_3 move within the entire range of Q max without considering the singularity. However, because actuators A_1, A_2, and A_3 move on the same axis, the intersection of the actuators is excluded, which is expressed as

$$q_{\min} < q_1 < q_3, \quad q_3 < q_2 < q_{\max}. \tag{18}$$

To prevent imaginary solutions in the inverse kinematics, the discriminant in the root must always be greater than zero. This constraint equation is expressed as

$$l^2 - (y - b\sin\theta)^2 > 0, \quad l^2 - (y + b\sin\theta)^2 > 0. \tag{19}$$

By plotting q_1, q_2, and q_3 to satisfy all aforementioned constraint equations, the following workspace (shown in Figure 6) is defined. In this case, the l link length is 250 mm and the b link length is 450 mm.

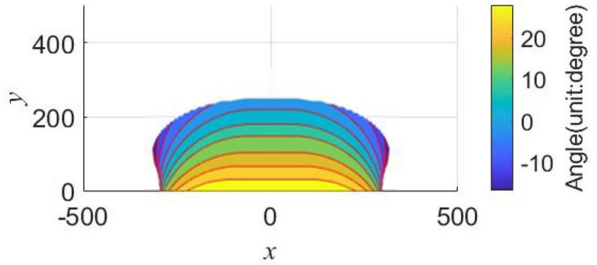

FIGURE 6. Theoretical workspace shown with the *x* and *y* position and the angle of the end effector.

B. SINGULARITY ANALYSIS

Both the **A** and **B** matrices obtained by the preceding Jacobian analysis can become singular at a certain position. Figure 7 shows the singular positions of the proposed manipulator. Because the generation of singularities causes a problem in lowering the DOF of the manipulator at this position, ensuring a non-singular area in the workspace is important. Therefore, we avoid cases such as those shown in Figure 7 by excluding the singular position in the theoretical workspace by ensuring that the determinant of the Jacobian matrix is zero. The cases are as follows: a) each side of the link is completely folded, b) the left link is in line with the end effector, c) the end effector is fully stretched, and d) The right link is in line with the end effector.

The q_1, q_2, and q_3 cannot intersect with one another because of the structure of the manipulator in which the three actuators move on a single ball screw. Therefore, in a situation where the length of half of the end effector is longer than the link, case "a)" in Figure 7 represents the initial position, and the position conditions are expressed as follows:

$$l = C_1, \quad b = C_1 + C_2, \; y = 0, \; q_3 = C_3, \; q_1 = q_3 - b + l, \; q_2 = q_3 + b - l, \quad \theta = 0, \quad (C_n \geq 0, \, C_n \text{ are random constant}). \tag{20}$$

Substituting Eq. (20) into Eqs. (15) and (16) yields the Jacobian matrix as follows:

$$\mathrm{A} = \begin{bmatrix} 2C_1 & 0 & -2C_1 \\ 0 & 2C_1 & -2C_1 \\ 0 & 0 & 1 \end{bmatrix}, \quad \mathrm{B} = \begin{bmatrix} 0 & 0 & 0 \\ 0 & 0 & 0 \\ 1 & 0 & 0 \end{bmatrix}, \quad \mathrm{J} = \begin{bmatrix} 1 & 0 & 0 \\ 1 & 0 & 0 \\ 1 & 0 & 0 \end{bmatrix}, \quad \det(\mathbf{J}) = 0. \tag{21}$$

Therefore, we can confirm that case "a)" in Figure 7 is a singular position.

In the same manner, the position conditions for case "c)" in Figure 7 are expressed as follows:

$$l = C_1, \quad b = C_1 + C_2, \; y = l, \; q_3 = C_3, \; q_1 = q_3 - b, \; q_2 = q_3 + b, \quad \theta = 0, \quad (C_n \geq 0, \, C_n \text{ are random constant}). \tag{22}$$

Substituting Eq. (22) into Eqs. (15) and (16) yields the Jacobian matrix as follows:

$$\mathrm{A} = \begin{bmatrix} 0 & 0 & 0 \\ 0 & 0 & 0 \\ 0 & 0 & 1 \end{bmatrix}, \quad \mathrm{B} = \begin{bmatrix} 0 & -2C_1 & C_1(2C_1+2C_2) \\ 0 & 2C_1 & C_1(2C_1+2C_2) \\ 1 & 0 & 0 \end{bmatrix}. \tag{23}$$

Therefore, matrix **A** has no inverse matrix. Because **J** cannot be defined, we can also confirm that case "c)" in Figure 7 is a singular position. In cases "b)" and "d)," moving from the actual robot is possible, but as presented in Section II-A, the movement of q_1 and q_2 is limited. Thus, these two cases are excluded.

IV. WORKSPACE OPTIMIZATION

In view of the application to facade cleaning of this 3-DOF parallel manipulator, a certain level of workspace must be ensured because the distance between the manipulator and outer wall must be kept constant during the cleaning process. Further, a workspace that is resistant to disturbance and can be moved must be provided. For this reason, a good condition workspace (GCW) is set as an index in this optimization process. More information can be found in the works of Liu et al. [24].

A. LOCAL CONDITIONING INDEX

The purpose of this optimization is to maximize the workspace of the manipulator under non-singular conditions. GCW is used to evaluate the degree of optimization. To define GCW, we need to define a local conditioning index (LCI). The condition number of the Jacobian matrix for defining LCI is

$$k = \left\|\mathbf{J}^{-1}\right\| \left\|\mathbf{J}\right\|. \tag{24}$$

The Euclidean norm of matrix $\|\cdot\|$ is defined as

$$\|\mathbf{J}\| = \sqrt{tr(\mathbf{J}^T\mathbf{W}\mathbf{J})}, \quad \mathbf{W} = \frac{1}{n}\mathbf{I}. \tag{25}$$

n denotes the dimension of the Jacobian matrix, and $\boldsymbol{\Pi}$ denotes an $n \times n$ identity matrix. The range of k should be $1 \leq k \leq \infty$.

The reciprocal of k has been used in several studies [25]–[28] to evaluate the accuracy and isotropy of the mechanism as LCI. Therefore, the present study also defines GCW based on LCI.

B. GOOD CONDITION WORKSPACE

When the workspace of the robot is analyzed based on the LCI, some points exist where the LCI values are extremely low. The higher the LCI value is, the better is the mechanism. Thus, locations where this index is low cannot be defined as good workspaces. Therefore, these locations should be excluded from the design process, and the remaining points can be referred to as points that belong to GCW. We define a set of points that is greater than or equal to a specific LCI value using GCW. Please see the Appendix for the previously mentioned Jacobian matrix and its corresponding condition number for this mechanism.

C. OPTIMIZATION RESULTS

The goal of this optimization process is to find the mechanism that has the largest workspace area with the highest GCW ratio among the workspaces of the manipulator according to the ratio of l and b for a given link length. Because the variables that affect the index are l and b, they are considered as design variables. The range of the initial and final values of the optimization simulation is determined according to the change limit in the length of the mechanism, as listed in Table 1.

TABLE 1. Range of the manipulator variables.

Parameter	Value range	Parameter	Value range
l	150–400 mm	b	300–550 mm

In the simulation, the link length is varied in units of 1 mm. As a representative example, six cases are considered by dividing the change in the link rate into 50-mm units, as shown in Figure 8, and the workspace of the proposed optimal model is shown in Figure 9.

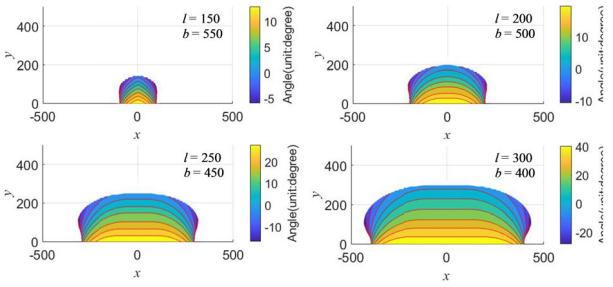

FIGURE 8. Four cases with 50-mm unit increment.

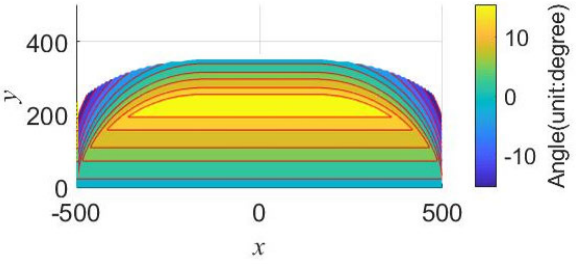

FIGURE 9. Optimized workspace with the l = 352 mm and b = 348 mm.

Based on the optimization, we can find the optimal kinematic parameter of $l = 352$ mm, and $b = 348$ mm, which can get workspace of 0.328 m^2 where almost all the workspace guarantees the good condition index. We used fmincon() function of MATLAB(2018, Mathworks). Table 2 lists the comparison of the optimization model with the previous six cases based on a major index.

V. PROTOTYPE AND EXPERIMENT

The purpose of this experiment is to verify whether a singular-free workspace obtained from the simulation can

TABLE 2. Comparison between the six cases and optimal model.

Case	l	b	Workspace area (m^2)	GCW ratio	Total GCW area (m^2)
1	150 mm	550 mm	0.025	78.8%	0.020
2	200 mm	500 mm	0.080	80.3%	0.064
3	250 mm	450 mm	0.153	83.4%	0.128
4	300 mm	400 mm	0.251	87.0%	0.217
optimal	*352 mm*	*348 mm*	*0.328*	*98.6%*	*0.323*

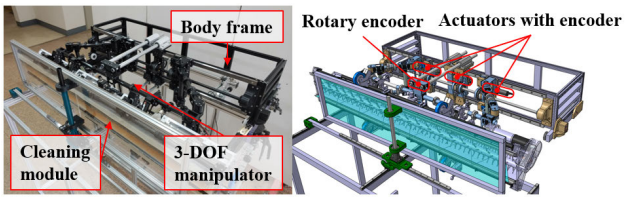

FIGURE 10. Sensor placement for the workspace measurement experiments.

TABLE 3. Hardware specifications of the manipulator.

Parameter	Value
Motor torque	54.5 mN·m
Gear head ratio	4.3:1
Material	Aluminum, Carbon polymer
Weight	25 kg
Volume	1280 mm × 610 mm × 320 mm

TABLE 4. Manipulator link parameters.

Parameter	Value	Parameter	Value
l	352 mm	b	348 mm
$q_{1\_initial\_position}$	100 mm	$q_{2\_initial\_position}$	100 mm
$q_{3\_initial\_position}$	0 mm		

be implemented in an actual mechanism. Experiments are performed using rotary and linear encoders to measure the motion of the actual end effector with respect to the motion of q_1, q_2, and q_3. The location-measurement results are compared with the theoretical workspace obtained from the simulations presented in Section III. They are analyzed to determine if a target workspace can be obtained. The arrangement of the sensors for the experiment is shown in Figure 10. The hardware specifications of the manipulator are listed in Table 3.

The link parameters of the manipulator, which are derived from the optimization process applied in the experiment, are listed in Table 4.

A. TEST RESULTS

The experimental results are shown in Figure 11. The figure shows the maximum 3-DOF movement, which illustrates how the actual workspace is implemented. The reason for the slightly narrower result than the area obtained by the simulation is that the experiment is performed by considering the collision and interference of the mechanism part, which are not considered in the simulation. Figure 12 shows the movement of the manipulator to compensate for the disturbance through the movement of each DOF. The following figures show that the mechanism, which has a non-singular workspace with high GCW, can be implemented. The detailed motion of the prototype is presented in the Multimedia extension.

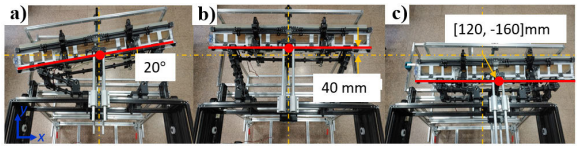

FIGURE 11. Manipulator maximum extended state and workspace, a) Maximum rotation of θ, b) Maximum extended state of the y axis, c) Maximum extended state of the x axis.

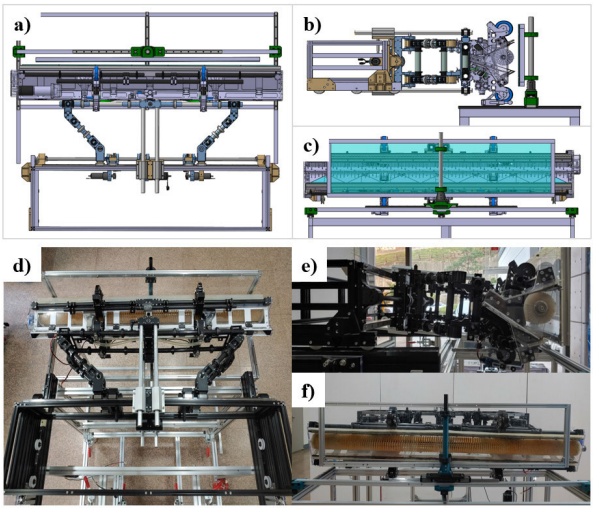

FIGURE 12. Disturbance compensation of manipulator, a and d) top view of the manipulator, b and e) side view of the manipulator, c and f) front view of the manipulator.

VI. CONCLUSION AND DISCUSSIONS

The existing 3-DOF manipulator is not suitable for facade cleaning. To solve this problem, the 3-DOF manipulator proposed in this paper adopted a single ball screw and a proposed linkage structure. The kinematic analysis and design parameters that define the workspace were also analyzed. From this analysis, the proposed 3-DOF manipulator was designed so that no singular position exists inside the workspace for facade cleaning. Further, according to the GCW index, we were able to establish a large workspace where the mechanism could achieve good performance. The manipulator, which takes advantage of the cleaning process when combined with the cleaning module, will be suitable for facade-cleaning robots.

There are some remaining controlling and sensing works to use this manipulator to compensate the disturbances. The y and θ directional disturbances in wall and yawing directions can be compensated by using position-based impedance control with disturbance observer technique [26]. The x directional disturbance, lateral direction of the gondola movement, is hard to measure. We are now developing a novel contact-based sensing device based on a parallel mechanism. By using the sensing device, the lateral disturbance can be simply compensated by a conventional regulator. We are going to share the compensation results in the near future.

$$\mathbf{J} = \begin{bmatrix} 1 & -(y - b\sin\theta)/(q_1 - q_3 + b\cos\theta) & (by\cos\theta + bq_1\sin\theta - bq_3\sin\theta)/(q_1 - q_3 + b\cos\theta) \\ 1 & (y + b\sin\theta)/(q_3 - q_2 + b\cos\theta) & (by\cos\theta + bq_2\sin\theta - bq_3\sin\theta)/(q_3 - q_2 + b\cos\theta) \\ 1 & 0 & 0 \end{bmatrix}$$

$$1/\left\{\left(\frac{(y+A_7)^2}{3A_{10}} + \frac{(y-vA_7)^2}{3A_{11}} + \frac{(A_4+A_3-A_1)^2}{3A_{11}} + \frac{(A_4+A_3-A_1)^2}{3A_{10}} + 1\right)^{\frac{1}{2}} * \left(\frac{(2q_3^2\sin\theta + q_1y\cos\theta + q_2y\cos\theta - 2q_3y\cos\theta + 2q_1q_2\sin\theta - 2q_1q_3\sin\theta - 2q_2q_3\sin\theta - bq_1\cos\theta\sin\theta + bq_2\cos\theta\sin\theta)^2}{A_9} + \frac{(q_1y - q_2y + 2by\cos\theta + A_3 + A_2 - 2bq_3\sin\theta)^2}{A_8} + \frac{A_{11}(A_6 + q_2\sin\theta - A_5)^2}{A_9} + \frac{A_{10}(A_6 + q_1\sin\theta - A_5)^2}{A_9} + \frac{A_{11}(y+A_7)^2}{A_8} + \frac{A_{10}(y-A_7)^2}{A_8} + \frac{1}{3}\right)^{\frac{1}{2}}\right\}$$

APPENDIX

[1] Jacobian matrix and the condition number of the mechanism are shown at the top of the this page, where

$$\begin{aligned}
A_1 &= bq_3\sin\theta \\
A_2 &= bq_2\sin\theta \\
A_3 &= bq_1\sin\theta \\
A_4 &= by\cos\theta \\
A_5 &= q_3\sin\theta \\
A_6 &= y\cos\theta \\
A_7 &= b\sin\theta \\
A_8 &= 3(b^2q_1\sin\theta - b^2q_2\sin\theta + 2by^2\cos\theta + bq_1y\sin\theta \\
&\quad + bq_2y\sin\theta - 2bq_3y\sin\theta)^2 \\
A_9 &= 3(2y^2\cos\theta + q_1y\sin\theta + q_2y\sin\theta - 2q_3y\sin\theta \\
&\quad + bq_1\sin\theta - bq_2\sin\theta)^2 \\
A_{10} &= (q_3 - q_2 + b\cos\theta)^2 \\
A_{11} &= (q_1 - q_3 + b\cos\theta)^2
\end{aligned}$$

REFERENCES

[1] SERBOT. *GEKKO Facade Robot*. Accessed: Jun. 4, 2019. [Online]. Available: https://www.serbot.ch/en/facade-cleaning/gekko-facade-robot

[2] Fraunhofer IFF. *SIRIUS Facade Cleaning Robot*. Accessed: Jun. 4, 2019. [Online]. Available: https://www.iff.fraunhofer.de/en/business-units/robotic-systems/facade-cleaning-sirius.html

[3] Skyprocy. *Cyprus*. Accessed: Jun. 4, 2019. [Online]. Available: http://www.skyprocy.com/

[4] N. Elkmann, M. Lucke, T. Krüger, D. Kunst, T. Stürze, and J. Hortig, "Kinematics, sensors and control of the fully automated facade cleaning robot siriusc for the fraunhofer headquarters buildung, munich," in *Proc. Adv. Climbing Walking Robots*, Jul. 2007, pp. 169–176.

[5] E. Gambao and M. Hernando, "Control system for a semi-automatic Façade cleaning robot," in *Proc. 23rd Int. Symp. Autom. Robot. Construction*, Oct. 2006.

[6] W. Wang, B. Tang, H. Zhang, and G. Zong, "Robotic cleaning system for glass facade of high-rise airport control tower," *Ind. Robot*, vol. 37, no. 5, pp. 469–478, Aug. 2010.

[7] T. Seo, Y. Jeon, C. Park, and J. Kim, "Survey on glass and Façade-cleaning robots: Climbing mechanisms, cleaning methods, and applications," *Int. J. Precis. Eng. Manuf.-Green Tech.*, vol. 6, no. 2, pp. 367–376, Apr. 2019.

[8] S. Yoo, I. Joo, J. Hong, C. Park, J. Kim, H. S. Kim, and T. Seo, "Unmanned high-rise Façade cleaning robot implemented on a gondola: Field test on 000-building in Korea," *IEEE Access*, vol. 7, pp. 30174–30184, 2019.

[9] J. Hong, G. Park, J. Lee, J. Kim, H. S. Kim, and T. Seo, "Performance comparison of adaptive mechanisms of cleaning module to overcome step–shaped obstacles on Façade," *IEEE Access*, vol. 7, pp. 159879–159887, 2019.

[10] H. Zhang, J. Zhang, W. Wang, R. Liu, and G. Zong, "A series of pneumatic glass-wall cleaning robots for high-rise buildings," *Ind. Robot*, vol. 34, no. 2, pp. 150–160, Mar. 2007.

[11] S.-M. Moon, D. Hong, S.-W. Kim, and S. Park, "Building wall maintenance robot based on built-in guide rail," in *Proc. IEEE Int. Conf. Ind. Technol.*, Mar. 2012, pp. 498–503.

[12] I. Joo, J. Hong, S. Yoo, J. Kim, H. S. Kim, and T. Seo, "Parallel 2-DoF manipulator for wall-cleaning applications," *Autom. Construct.*, vol. 101, pp. 209–217, May 2019.

[13] S. Kamada, T. Laliberte, and C. Gosselin, "Kinematic analysis of a 4-DOF parallel mechanism with large translational and orientational workspace," in *Proc. Int. Conf. Robot. Autom. (ICRA)*, May 2019, pp. 1637–1643.

[14] K. Wen, D. Harton, T. Laliberte, and C. Gosselin, "Kinematically redundant (6+3)-DoF hybrid parallel robot with large orientational workspace and remotely operated gripper," in *Proc. Int. Conf. Robot. Autom. (ICRA)*, May 2019, pp. 1672–1678.

[15] X.-J. Liu, J. Wang, and G. Pritschow, "Kinematics, singularity and workspace of planar 5R symmetrical parallel mechanisms," *Mechanism Mach. Theory*, vol. 41, no. 2, pp. 145–169, Feb. 2006.

[16] Y. Li and Q. Xu, "Kinematic analysis of a 3-PRS parallel manipulator," *Robot. Comput.-Integr. Manuf.*, vol. 23, no. 4, pp. 395–408, Aug. 2007.

[17] C. Gosselin, T. Laliberte, and A. Veillette, "Singularity–free kinematically redundant planar parallel mechanisms with unlimited rotational capability," *IEEE Trans. Robot.*, vol. 31, no. 2, pp. 457–467, Apr. 2015.

[18] L.-W. Tsai and S. Joshi, "kinematics and optimization of a spatial 3-UPU parallel manipulator," *J. Mech. Des.*, vol. 122, no. 4, pp. 439–446, Dec. 2000.

[19] J. Wu, J. Wang, and L. Wang, "Optimal kinematic design and application of a redundantly actuated 3dof planar parallel manipulator," *J. Mech. Des.*, vol. 130, no. 5, May 2008.

[20] M. Stock and K. Miller, "Optimal kinematic design of spatial parallel manipulators: Application to linear delta robot," *J. Mech. Des.*, vol. 125, no. 2, pp. 292–301, Jun. 2003.

[21] T. Harada and P. Liu, "Internal and external forces measurement of planar 3-DOF redundantly actuated parallel mechanism by axial force sensors," *ISRN Robot.*, vol. 2013, pp. 1–8, Oct. 2013.

[22] X.-J. Liu, F. Gao, J. Wang, and J. Li, "A new planar two degrees of freedom parallel mechanism," *IFAC Proc. Vol.*, vol. 34, no. 4, pp. 113–117, May 2001.

[23] *Strong Winds SLAM Cleaning Platform Into Shanghai Skyscraper*. Accessed: Jun. 4, 2019. [Online]. Available: https://www.youtube.com/watch?v=mL_LuxMWPl8&list=PLD0ZUNGYxKxawV176Xwao9t9YnqrEHoA7&index=38&t=0s

[24] X.-J. Liu, J. Wang, and G. Pritschow, "On the optimal kinematic design of the PRRRP 2-DoF parallel mechanism," *Mechanism Mach. Theory*, vol. 41, no. 9, pp. 1111–1130, Sep. 2006.

[25] G. Alici, "An inverse position analysis of five-bar planar parallel manipulators," *Robotica*, vol. 20, no. 2, pp. 195–201, Mar. 2002.

[26] X. J. Liu, "The relationships between the performance criteria and link lengths of the parallel manipulators and their design theory," Yanshan Univ., Qinhuangdao, China, Tech. Rep., 1999.
[27] F. Gao, X.-J. Liu, and X. Chen, "Relationships between the shapes of the workspaces and the link lengths of 3-DOF symmetrical planar parallel manipulators," *Mech. Mach. Thoery*, vol. 36, no. 2, pp. 205–220, 2001.
[28] C. A. Klein and B. E. Blaho, "Dexterity measures for the design and control of kinematically redundant manipulators," *Int. J. Robot. Res.*, vol. 6, no. 2, pp. 72–83, Jun. 1987.

GARAM PARK received the B.S. degree in mechanical engineering from Hanyang University, South Korea, in 2019. He is currently working pursuing the M.S. degree in mechanical engineering with Hanyang University. His research interest includes robot mechanism design.

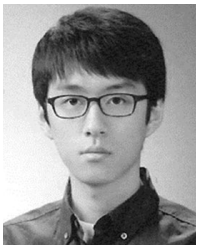

JOOYOUNG HONG received the B.S. degree in mechanical engineering from Yonsei University, South Korea, in 2018. He is currently pursuing the M.S. degree in mechanical engineering with Seoul National University, South Korea. His research interest includes robot mechanism design.

SUNGKEUN YOO received the B.S. degree in mechanical and aerospace engineering from Seoul National University, South Korea, in 2014, where he is currently pursuing the Ph.D. degree in mechanical engineering. His research interest includes robot mechanism design.

HWA SOO KIM (Member, IEEE) received the B.S. and Ph.D. degrees in mechanical engineering from Seoul National University, South Korea, in 2000 and 2006, respectively. He is currently an Associate Professor with the Department of Mechanical System Engineering, Kyonggi University, South Korea. From 2007 to 2008, he was a Postdoctoral Researcher with the Laboratory for Innovations in Sensing, Estimation and Control, University of Minnesota, MN, USA. His current research interests include design, modeling, and control of various mobile platforms.

TAEWON SEO (Member, IEEE) received the B.S. and Ph.D. degrees from the School of Mechanical and Aerospace Engineering, Seoul National University, South Korea. He was a Postdoctoral Researcher with the Nanorobotics Laboratory, Carnegie Mellon University, an Visiting Professor with the Biomimetic Millisystems Laboratory, University of California, Berkeley, and an Assistant Professor with the School of Mechanical Engineering, Yeungnam University, South Korea. He is currently an Associate Professor with the School of Mechanical Engineering, Hanyang University, South Korea. His research interests include robot design, analysis, control, optimization, and planning. He received the Best Paper Award of the IEEE/ASME TRANSACTION ON MECHATRONICS, in 2014. He is also a Technical Editor of IEEE/ASME TRANSACTION ON MECHATRONICS and an Associate Editor of the IEEE ROBOTICS AND AUTOMATION LETTERS and *Intelligent Service Robots*.